IIETA International Information and Engineering Technology Association
Advancing the World of Information and Engineering

Mathematical Modelling of Engineering Problems
Vol. 11, No. 10, October, 2024, pp. 2731-2739
Journal homepage: http://iieta.org/journals/mmep

Role of Heat Carrier Components in the Formation of Corrosion and Scale Deposits in the Pipes of Heat Supply Systems

Balzhan Kabylbekova[1], Nadezhda Vysotskaya[1], Abibulla Anarbayev[2], Roza Spabekova[3], Karim Kurbanbekov[1], Zhakhongir Khussanov[4*], Gulnur Kaldybekova[5]

[1] Chemistry and Pharmaceutical Engineering Department, M. Auezov South Kazakhstan State University, Shymkent 160012, Kazakhstan
[2] Technology of Inorganic and Petrochemical Industries Department, M. Auezov South Kazakhstan State University, Shymkent 160012, Kazakhstan
[3] Physics Department, M. Auezov South Kazakhstan State University, Shymkent 160012, Kazakhstan
[4] Testing Regional Laboratory of Engineering Profile Structural and Biochemical Materials, M. Auezov South Kazakhstan State University, Shymkent 160012, Kazakhstan
[5] Department of Biotechnology, M. Auezov South Kazakhstan State University, Shymkent 160012, Kazakhstan

Corresponding Author Email: zhakhangir@mail.ru

https://doi.org/10.18280/mmep.111015

Received: 2 August 2024
Revised: 3 October 2024
Accepted: 10 October 2024
Available online: 31 October 2024

Keywords:
corrosion and scale deposit, heat carrier, carbon dioxide equilibrium

ABSTRACT

The problem of heat carrier (water) components affecting the inner surface of steel equipment in heat supply systems is complex and associated with various factors. Chemically complex water with dissolved gases and microorganisms can form corrosion and scale deposits composed of carbonates, silicates, sulfates, and alkali metal sulfides. The disruption of carbon dioxide equilibrium in water leads to the formation of dense or loose deposits on the inner metal surfaces, which impede heat carrier circulation, thereby slowing its supply to the consumer. To resolve the arising problems with the heat carrier, the authors explore and establish the components of water from different wells in the studied region using chemical analysis and mass spectroscopy, reporting on their qualitative and quantitative characteristics with units of measurement. A detailed description of the corrosion and scale deposits formed by the heat carrier is prepared using a JSM-6490LV scanning electron microscope with INSAEnergu energy-efficiency microanalysis systems and HKL basic structural analysis with an ×300,000 useful magnification combined with a highly effective liquid chromatograph Varian ProStar.

1. INTRODUCTION

Water from natural open and underground sources used as a heat carrier in heat supply systems is a solution of mineral salts and gases. Solutions are subjected to treatment to be used for industrial purposes as heat carriers. If the heat carrier contains dissolved oxygen, sulfates, nitrites, and carbonic acid due to the thermal decomposition of carbonates and hydrocarbonates, the inner surface of pipes in heating systems can be subjected to corrosion [1-3].

Water becomes enriched with dissolved substances as a result of contact with rock, which determines its chemical composition. The totality of mineral salts, organic substances, and gases dissolved in water determines its quality and treatment for use in industrial and residential facilities. pH and hardness are important for water industrial use, while corrosion aggressiveness is determined by calcium, magnesium, iron, and silicon ions.

Numerous selected and tested methods of heat carrier processing prevent the formation of corrosion and scale deposits (CSDs) on the inner surface of equipment, including specialized inhibitors and surfactants. The corrosion of heat supply equipment is prevented using corrosion-resistant metals, protective coatings on the metal surface (hot dip galvanizing, oxidation, metal spraying), deaeration and decarbonization of the heat carrier, silicate treatment of the heat carrier, compositions of organic colloids (gelatin, carpenter's glue), amines, and their salts [4-7].

The development of effective methods to combat corrosion damage on the inner surface of heat supply pipes is justified by the choice of economic and technological protection methods [8]. Boiler sludge oversaturates the heat carrier with Ca^{2+} and Mg^{2+} ions, leading to the emergence of the first foci of the solid phase in the form of numerous centers of crystallizing salt, which then grow from submicroscopic to microscopic and merge into a crystalline state of scale. To remove the resulting scale, reference [8] used repeated circulation of wash solutions through the system, employing a mixture of hydrochloric acid solutions with the addition of urotropin.

Solutions for cleaning pipelines from scale deposits that are effective, environmentally friendly, and easily decomposed

and consumed by microbiota include mixtures of citric acid with mineral and citric acids (78%) and tartaric acid with polyethylene glycol. Citrate ions are diluted in a solution to a concentration of 4-8% at 60-80°C. Effective use is facilitated by tablets that easily dissolve in water [9, 10].

A factor reducing the effectiveness of heat supply systems is the deposition of corrosion products in the form of iron oxides and hydroxides. These compounds form on the inner surface of heat exchangers and pipelines in heat supply systems that use highly mineralized heat carriers. These factors affect heat transfer and the system's hydraulic resistance. Wash solutions, such as mixtures of citric and hydrochloric acids with chitosan modified with isobutyric acid, eliminate the negative impact of corrosion on heat transfer [11].

The composition of the EPAM cationic polyelectrolyte, which is a water-soluble amino-epichlorohydrin copolymer containing cationic groups with ammonia, inhibitor-gel-like tertiary aliphatic amine, and nitrobenzene-sulfonic acids, is used to reduce corrosion of steel equipment in heating systems [12, 13].

Inhibitor substances in the composition of the heat carrier prevent the formation of CSDs in closed heating systems. Detergents based on boron-sulfamic acid (40-50 g/l) with thiosemicarbonate (0.2-0.8 g/l) and organoboron compounds prove effective, showing a comprehensive effect. At high temperatures, the positive effect of such complexes is reduced due to the formation of a mushy mass, hindering the circulation of the coolant and reducing the cleaning rate [14, 15].

Based on an analytical review of organoboron compounds, the ability of amino borates to protect steel equipment in heat supply systems compared to the protective capabilities of simple amines and boric acid is attributed to the ability to form a strong adsorption film on the steel surface preventing corrosion [16, 17].

Several studies [18, 19] describe the current state of corrosion of steel equipment in acidic media. Effective protection against corrosion is provided by organic molecules in a solution capable of chemisorption interaction with the steel surface and forming polymolecular protective layers of chemically bonded molecules on its surface. The effects of inhibitors in hot solutions of organic acids are demonstrated.

An interesting innovation to prevent scale accumulation is current-carrying electric potential (CCEP), produced by a converter with a frequency transformer and a potential regulator. CCEP can be applied to any part of the metal pipe surface for varying periods and ranges from 10 to 200 V. This device does not require additional treatment reagents, which makes it environmentally friendly. It eliminates additional water-softening costs [20].

Although significant research has been conducted on methods to prevent corrosion and scale deposition (CSD) in heat supply systems, a gap exists in understanding the role of mineral content variability across different water sources and its direct impact on CSD formation. While numerous studies have explored the effects of chemical inhibitors, surfactants, and advanced treatment techniques, there is limited investigation into how different mineral concentrations, specifically calcium, magnesium, and sulfates, influence CSD accumulation and the efficiency of preventive measures across various regions and water wells. Additionally, the interplay between environmental factors, such as temperature fluctuations and the chemical composition of local water sources, on the long-term performance of corrosion inhibitors and scale preventers remains underexplored.

This research seeks to bridge this gap by focusing on the comparative analysis of water from different wells and their specific mineral compositions to evaluate their role in CSD formation on steel surfaces. The study aims to establish the role of indicators forming CSDs on the metal surface of the pipe in water samples from different wells.

It is hypothesized that water from different wells, with varying concentrations of minerals such as calcium, magnesium, and sulfates, plays a significant role in CSD formation on the inner surfaces of steel pipes. Furthermore, it is expected that the application of chemical inhibitors, along with other treatment methods, will effectively reduce corrosion and scale deposition, thereby enhancing system efficiency and minimizing energy losses.

2. METHODS

The study was conducted from October 27 to November 1, 2023 in the Turkistan region, Kazakhstan. The composition of water from the Tassai, Aikol, Dostyk, and Eltai wells in the Turkistan region and the city of Shymkent was established by chemical analysis.

To determine the composition of the source water, we took 5.0 dm^3 samples from each well. A total of 12 samples (three from each well) were taken to ensure a representative dataset. For each sample, we conducted three replicates of every test, and the results were averaged to enhance the reliability of the measurements.

The samples were chemically analyzed to determine the quantitative content of metal and nonmetal ions no later than 6 hours after sample collection.

The pH of the water was measured electrometrically using a pH meter calibrated with standard buffer solutions (pH 4.0, 7.0, and 10.0).

To determine dry residue, we placed a known volume of water in a porcelain cup and evaporated it at 100-110°C. The contents of the cup were then dried in a drying cabinet at 160°C for 1-2 hours, transferred to a desiccator, cooled to 20-25°C, and weighed, after which dry residue was calculated using the formula:

$$X1 = \frac{(m_1 - m_2) * 1{,}000}{V} \quad (1)$$

where,

m_1 – the mass of the cup with the evaporated test solution,

m_2 – the mass of the cup without the test solution,

V – the volume of water taken for analysis.

The total alkalinity of the water samples was determined titrimetrically. The water was placed into a 100 ml conical flask using a 25 ml pipette, 2-4 drops of 0.1% methyl orange solution were added, and the sample was titrated with 0.1 n. hydrochloric acid HCl solution with constant stirring until the yellow color of the solution changes to slightly pink. The total alkalinity was calculated using the formula:

$$X2 = \frac{V * N * 1{,}000}{V_1} \text{ mg/l} \quad (2)$$

where,

V – the volume of hydrochloric acid solution consumed for

titration, ml,

N – normality of the hydrochloric acid solution,

V_1 – the volume of the tested water, ml.

Calcium ions. We placed the tested water containing 2-20 mg of calcium in a conical flask, added 90-100 cm^3 of distilled water, 2 cm^3 of sodium hydroxide solution, and 0.2-0.3 g of murexide (pH 10.8-13.2), and titrated with the Trilon B solution until the color changed from pinkish red to violet.

$$X3 = \frac{(V_1 * 0.0010 * 1{,}000 * 100)}{V} \quad (3)$$

where,

V_1 – the volume of Trilon B used for calcium titration, cm^3,

0.0010 – the mass of calcium equivalent to the mass of Trilon B in 1 cm^3 of the solution with the molar concentration of the equivalent at 0.05 mol/dm^3, g,

1000 – the factor to convert grams to milligrams,

100 – the factor to account for dilution and concentration units,

V – the volume of the solution taken for analysis, cm^3.

Magnesium ions in the presence of calcium. The calcium and magnesium sum were titrated with Trilon B in the presence of an ammonium-ammonia buffer solution (9-10 pH) with the Eriochrome Black indicator. The amount of Trilon B used for calcium determination was considered when processing the results. The method was applied to determine a magnesium mass concentration of 20 mg/dm^3 and higher. The lower detection limit was 2.0 mg/dm^3.

$$X4 = \frac{(V_2 - V_1) * 0.0006 * 1{,}000 * 1{,}000}{V} \quad (4)$$

where,

V_1 – the volume of Trilon B used for calcium titration, cm^3,

V_2 – the volume of Trilon B used for calcium and magnesium titration, cm^3,

0.0006 – the mass of magnesium equivalent to the mass of Trilon B in 1 cm^3 of the solution with the molar concentration of the equivalent at 0.05 mol/dm^3, g,

V – the volume of water taken for analysis, cm^3.

Total hardness. The total hardness was determined based on calcium and magnesium ions. The hardness of water is the sum of calcium and magnesium ions.

$$H_{total} = X_3 + X_4 \quad (5)$$

where,

H_{total} – the total hardness,

X_3 – the amount of calcium ions,

X_4 – the amount of magnesium ions.

Qualitative and quantitative composition of scale deposits. The composition of CSD formed by the water on the surface of metal pipes was determined using a JSM-6_{490}LV scanning electron microscope with INSAEnergu energy-efficiency microanalysis systems and HKL basic structural analysis with a ×300,000 useful magnification combined with a highly effective liquid chromatograph VarianProStar. The electron microscope enabled qualitative and quantitative analysis of the scale deposit, which stimulates general and local corrosion resulting in the destruction of the pipe, boiler, heat exchanger, and radiator and an 8-10% over expenditure of electricity during operation in the presence of 2 mm thick scale deposit in the system. ×300,000 useful magnification combined with the highly effective liquid chromatograph Varian ProStar allowed us to identify impurities and inclusions in the samples in percentage by weight and to see their structure.

To further ensure the reliability of the data, we conducted duplicate analyses on a subset of the samples. These duplicate analyses consistently produced results within 2% of the original measurements, further confirming the precision and reproducibility of the methods used.

All equipment used for chemical and spectroscopic analysis was calibrated against internationally recognized standards. For mass spectroscopy, the instrument was calibrated using a NIST traceable multi-element standard solution (HI70032P) to ensure the accuracy of elemental concentration measurements. The reproducibility of the results was confirmed by analyzing duplicate samples and conducting blank tests.

3. RESULTS

Data describing the water samples from different wells are provided in Tables 1-5.

Table 1 contains the composition indicators of water from different wells: well №1 – network water for household purposes and residential areas; wells №2 and 3 – water from an industrial zone, 5, 10, and 15 km, respectively, used for technical purposes; well №4 – drinking water.

Table 1. Water composition indicator

Indicator, Units of Measurement	Well №1	Well №2	Well №3	Well №4
Dry residue, mg/dm^2	235	258	319	270
Total hardness, mg-eq/dm^2	1.05	4.06	5.56	8.5
Electrical conductivity, µS/cm	333	495	619	504
Potential of hydrogen, pH	7.05	8.29	8.09	8.33
Amount of Cl^-, mg/dm^3	12	1.04	-	168
Amount of SO_4^{2-}, mg/dm^3	1.2	9.24	11.92	-
Amount of Mg^{2+}, mg/dm^3	3.9	17.25	28.5	22.5
Amount of Ca^{2+}, mg/dm^3	3.8	52.5	55	55
Amount of Si^+, mg/dm^3	0.6	3.27	11.51	-
Amount of Fe^{2+}, mg/dm^3	-	0.94	-	-
Amount of Na^+, mg/dm^3	40	5.96	-	3.68
Amount of K^+, mg/dm^3	0.9	3.30	-	-
Amount of Pb^{2+}, mg/dm^3	-	0.01	0.01	0.01
Amount of Cd^{2+}, mg/dm^3	-	0.001	0.0009	0.001
Amount of Cu^{2+}, mg/dm^3	-	0.65	0.58	0.65
Amount of As^{3+}, mg/dm^3	-	0.004	0.002	0.004
Amount of Sn^{2+}, mg/dm^3	-	11.01	17.95	-
Amount of Sb^{2+}, mg/dm^3	-	35.93	58.58	-
Amount of J^+, mg/dm^3	-	9.64	15.71	-
Amount of NH_4^+, mg/dm^3	-	0.2	0.1	0.1

The composition of water from wells №2 and 3 differed slightly in terms of the assessed indicators. The water from well №4 differed by the content of magnesium and chlorine ions. Sulfate, calcium, and magnesium ions, capable of producing scale, were found in sufficient quantities. Heat carriers containing these ions in the composition of water are more capable of forming scale on the inner surfaces of metal equipment.

Table 2 presents water component indicators for:

Wells №1 and 2 – industrial zone, 5 km,

Wells №3 and 4 – industrial zone, 15 km

The content of iron, sulfate, calcium, and magnesium ions was the highest in well №2. Similar to well №1, water containing the ions is more capable of forming scale on the metal surfaces of the equipment supplying the heat carrier (water) to the consumer.

Table 2. Water composition indicator

Indicator, Units of Measurement	Well №1	Well №2	Well №3	Well №4
Dry residue, mg/dm^2	818	1,501	40	85
Total hardness, mg-eq/dm^2	10.42	22.22	1.92	3.84
Electrical conductivity, μS/cm	1,011	453	545	468
Potential of hydrogen, pH	7.43	7.78	8.32	8
Smell at 20ºC, points	0	0	0	0
Color, degrees (norm – 35)	10	-	-	-
Turbidity, mg/l (Kaolin standard 2)	0.5	0.5	-	-
Amount of Cl^- ions, mg/dm^3	49.52	505	-	-
Amount of SO_4^{2-} ions, mg/dm^3	15	490	-	9.24
Amount of Mg^{2+} ions, mg/l	69	156.6	15	15.75
Amount of Ca^{2+} ions, mg/dm^3	105	202	15	53.75
Amount of Si^+ ions, mg/l	0.079	129.7	24.8	9.36
Amount of Fe^{3+} ions, mg/dm^3	0.1	11.21	0.3	0.14
Amount of Na^+ ions, mg/l	0.38	402.5	-	4.45
Amount of K^+ ions, mg/l	0.14	-	-	-
Amount of Pb^{2+} ions, mg/dm^3	0.01	0.01	0.01	0.025
Amount of Cd^{2+} ions, mg/dm^3	0.0009	0.001	0.009	0.0001
Amount of Cu^{2+} ions, mg/dm^3	0.2	0.7	0.78	0.088
Amount of As^{3+} ions, mg/dm^3	0.1	0.005	0.008	0.0003
Amount of NH_4^+ ions, mg/dm^3	0.1	0.2	0.1	-
Permanganate oxidation, mg/l	0.23	0.13	-	-
Total microbial count, bacteria/1 ml	-	136	49	30
Total microbial count, bacteria.100 ml	-	240	-	-

Table 3 describes the composition of water from the Maiatal well, located near the industrial Kainar LLC plant, processing phosphorus industry waste.

Table 3. Water composition indicators

Indicator	Factual Results, mg/l
pH	7.22
Total hardness, mg-eq/l or mol/l	14; 7.0
SO_4^{2-} ions	0.09
Cl^- ions	0.03
Na^+ ions	6.3
K^+ ions	2.28
Mg^{2+} ions	31
Al^{3+} ions	0.02
Ca^{2+} ions	139
Ti^{4+} ions	0.0014
Cr^{3+} ions	0.0033
Mn^{2+} ions	0.0002
Fe^{3+} ions	3.0
Co^{3+} ions	0.0005
Rb^+ ions	0.0013
Zr^+ ions	0.0001
Sr^{2+} ions	0.756
Mo^{3+} ions	0.0011
Cd^{2+} ions	0.0001
Sn^{2+} ions	0.0001
Sb^{3+} ions	0.0001
Ba^{2+} ions	0.0318
U^+ ions	0.0037
Cu^{2+} ions	0.0088

Analyzing the composition of water from the well near the industrial zone, we noted significant amounts of calcium (139 mg/l) and magnesium (31 mg/l) ions. This amount of calcium and magnesium ions can form scale compounds on the metal surface of pipes when this water is used as a heat carrier. Significant amounts of other ions, while their content in water remains insignificant, do not play any role in the formation of scale.

Summarizing the data on the composition of water from different wells, it is possible to competently choose an effective inhibitor to protect the surface of pipes from corrosion damage.

Figures 1-3 show the results of the analysis of corrosion scale on metal pipes and the composition of scale by individual components.

Figure 1 shows the components of the CSD formed by the heat carrier on the inner surface of a metal pipe from well №2.

Based on Figure 1, the CSD on the inner surface of the heat carrier supply pipe contained Ca and Mg.

Figure 2 shows the characteristics of the components of the CSD on the inner surface of a metal pipe from well №3.

Figure 2 shows a dark corrosion and scale formation on the inner surface of the pipe, formed by a heat carrier containing significant amounts of Ca and Mg.

Figure 3 presents the values of corrosion and scale components formed on the inner surface of a metal pipe by the heat carrier from the well characterized in Table 3, located 10 km away from an industrial facility dealing with the processing and disposal of phosphorus slag.

Figure 3 shows a gray CSD on the inner surface of the pipe

supplying the heat carrier from the well located 15 km away from the industrial facility. Comparing the composition of the CSD shown in Figure 3 with the deposit in Figure 2, we noted a significantly lower content of Ca and Mg ions.

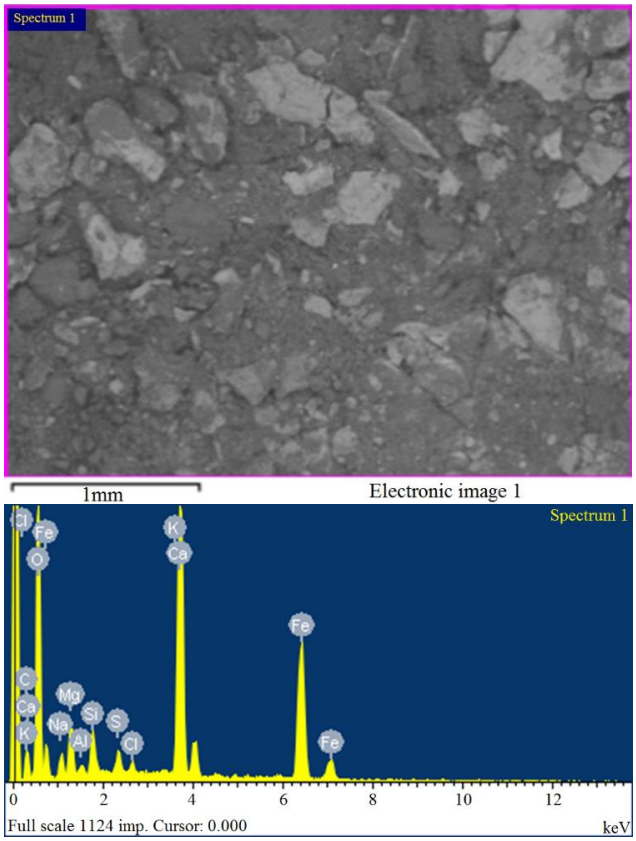

Element, Weight (%): C, 11.33; O, 42.34; Na, 2.23; Mg, 2.96; Al, 0.38; Si, 1.56; S, 0.85; Cl, 0.44; K, 0.22; Ca, 16.17; Fe, 21.51; Total, 100.00

Figure 1. CSD on the inner surface of the pipe formed by the heat carrier in well №2

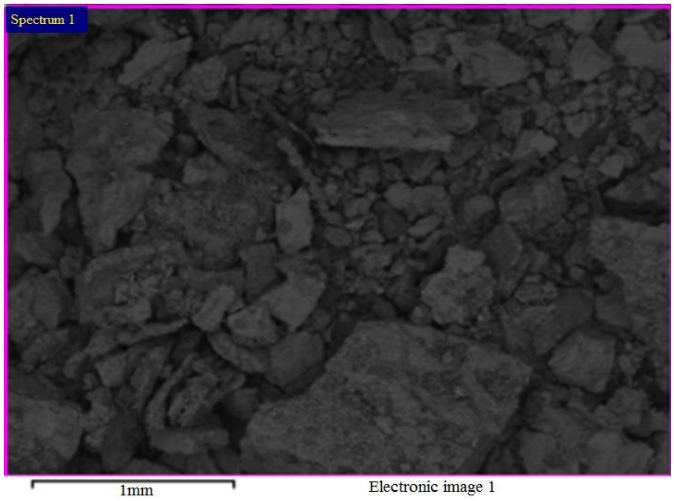

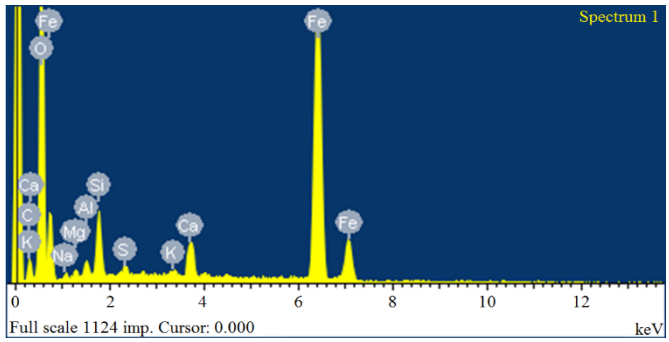

Element, Weight (%): C, 6.61; O, 24.49; Na, 0.75; Mg, 2.45; Al, 0.85; Si, 3.00; S, 0.37; K, 0.27; Ca, 12.29; Fe, 48.93

Figure 2. CSD on the inner surface of the pipe formed by the heat carrier in well №3

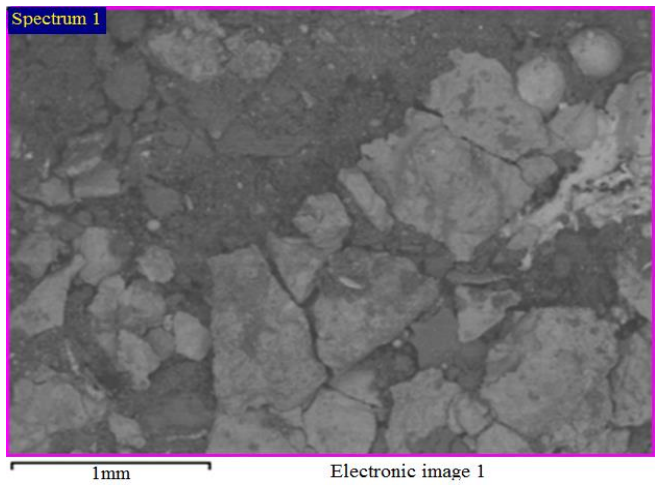

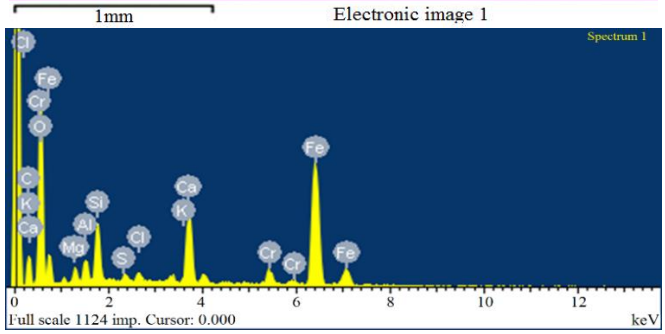

Element, Weight (%): C, 19.67; O, 34.93; Mg, 1.31; Al, 1.50; Si, 3.53; S, 0.30; Cl, 0.74; K, 0.54; Ca, 5.84; Cr, 2.17; Fe, 29.47; Total, 100.00

Figure 3. CSD on the inner surface of the pipe formed by the heat carrier in the well at a distance of 10 km

Examining the water of water and heat supply systems from underground wells, we observed various components.

Table 4 shows the composition of water from the Tassai reservoir wells (industrial zone wells №1 and 2) and water from filter №3 10-15 km away from the industrial zone producing mineral fertilizers.

Table 4. Water composition indicators

Indicator, Units of Measurement	Well №1	Well №2	Well №3
Dry residue, mg/l	290	249	244
Total hardness, mg-eq/dm^2	6.08	3.8	3.6
Electrical conductivity, µS/cm	677	447	417
Potential of hydrogen, pH	6.74	8.47	7.4
Permanganate oxidation, mg/l	290	0.23	0.23
Oil products, total	6.08	not found	not found
Phenol, mg/l	677	not found	not found

Indicator, Units of Measurement	Well №1	Well №2	Well №3
Synthetic surfactants, mg/l	0.37	not found	not found
Amount of Cl^- ions, mg/dm^3	not found	1.9	1.07
Amount of SO_4^{2-} ions, mg/dm^3	not found	8.2	7.36
Amount of Mg^{2+} ions, mg/dm^3	not found	16.4	12.0
Amount of Ca^{2+} ions, mg/dm^3	1.64	78.4	84
Amount of Si^+ ions mg/dm^3	12.94	1.6	1.75
Amount of Na^+ ions, mg/dm^3	36	7.2	4.2
Amount of K^+ ions, mg/dm^3	95.2	0.2	0.2

Figure 4 shows the CSD formed by the heat carrier (water) in a well at a distance of 15 km (Table 4).

Figure 5 shows the formation of CSDs on the inner surface of a metal pipe in well №2 (Table 4) 10 km from the industrial area.

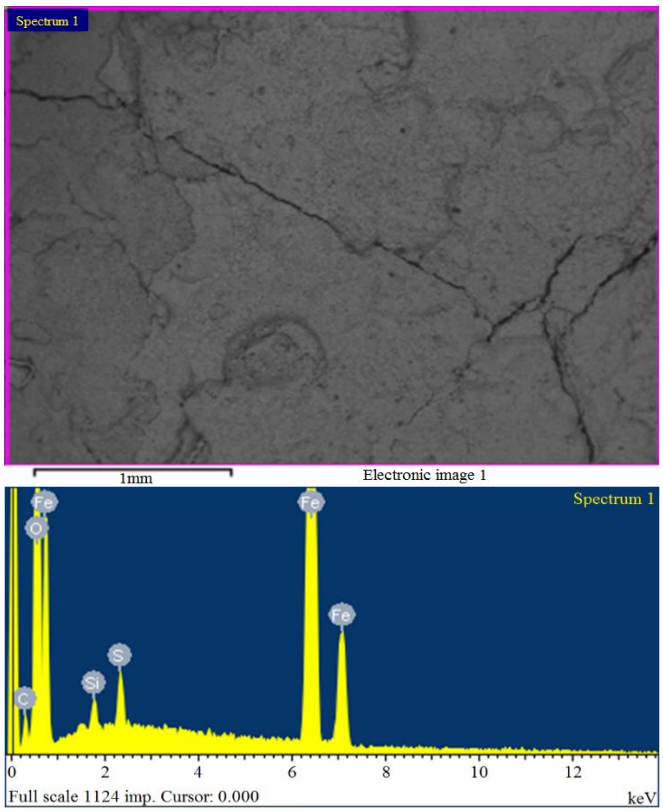

Element, Weight (%): C, 3.80; O, 32.59; Si, 0.60; S, 1.07; Ca, 1.07; Mg, 21.3; Fe, 25.4; Total, 15.24

Figure 4. CSD on the inner surface of the pipe formed by the heat carrier in well №1

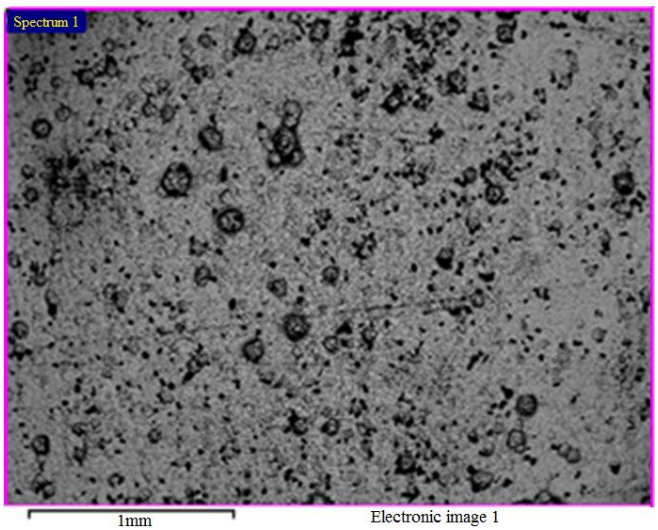

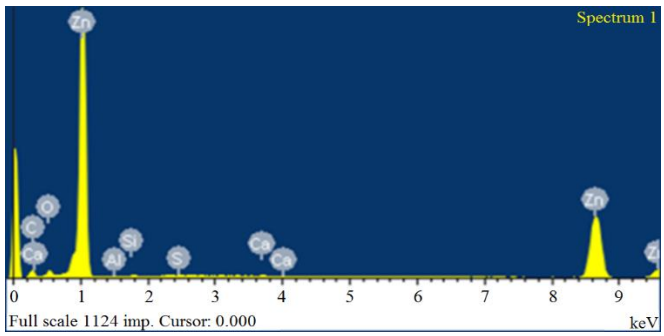

Element, Weight (%): C, 4.10; O, 29.6; Si, 3.90; S, 2.51; Ca, 17.9; Mg, 21.6; Fe, 20.39; Total, 100.00

Figure 5. CSD on the inner surface of the pipe formed by the heat carrier in well №2 at a distance of 10 km

Table 5 summarizes the composition of water taken from the wells near the agrarian complex (greenhouse).

The chemical analysis of water from the different wells (Tables 1-5) revealed significant variability in key ion concentrations that are directly related to corrosion and scale deposition (CSD). Notably, water from wells №2 and №3 exhibited higher levels of calcium (52.5 mg/dm³ and 55 mg/dm³, respectively) and magnesium ions (17.25 mg/dm³ and 28.5 mg/dm³) compared to well №1 (Ca: 3.8 mg/dm³; Mg: 3.9 mg/dm³). These elevated concentrations suggest a greater potential for scale formation in wells №2 and №3.

Table 5. Water composition indicators

Indicator, Units of Measurement	Well №1	Well №2	Well №3
Dry residue, mg/dm^2	354	682	858
Total hardness, mol/dm^2	5.1	9.5	10.6
Electrical conductivity, µS/cm	608	1,022	1,194
Potential of hydrogen, pH	8.21	7.64	7.72
Amount of Cl^-, mg/l	1.04	-	168
Amount of SO_4^{2-}, mg/l	52.89	197	57.36
Amount of Mg^{2+}, mg/l	26.4	66	62.4
Amount of Ca^{2+}, mg/l	58	80	108
Amount of Si^+, mg/l	9.35	2.73	1.75
Amount of PO_4^{3-}	0.031	0.032	0.036
Amount of Na^+, mg/l	5.96	52.46	16.94
Amount of K^+, mg/l	1.29	1.55	-
Amount of Pb^{2+}, mg/dm^3	0.028	0.02	0.02
Amount of Cd^{2+}, mg/dm^3	0.001	0.001	0.001
Amount of Cu^{2+}, mg/dm^3	0.5	0.3	0.3
Amount of As^{3+}, mg/dm^3	0.03	0.04	0.03
Amount of NH_4^+, mg/l	0.2	0.2	0.1

Additionally, well №4 showed the highest concentration of chlorine ions (168 mg/dm³) and magnesium ions (22.5 mg/dm³), further indicating a higher likelihood of both scale and corrosion. This contrasts with well №1, which had relatively low levels of chlorine (12 mg/dm³) and magnesium ions (3.9 mg/dm³), implying less aggressive water quality.

Electrical conductivity also varied significantly between the wells, with well №3 showing the highest value (619 µS/cm), further indicating its higher ion concentration and, consequently, a higher likelihood of deposit formation. In contrast, well №1 exhibited the lowest electrical conductivity (333 µS/cm), corresponding to its lower ion content.

In addition to calcium, magnesium, and silicon ions, water from each well also contained insignificant amounts of PO43- ions, which were not observed in the composition of water from previous wells.

Figure 6 shows CSD on the inner surface of a metal pipe formed by water from well №3 (Table 5) 3 km away from the greenhouse.

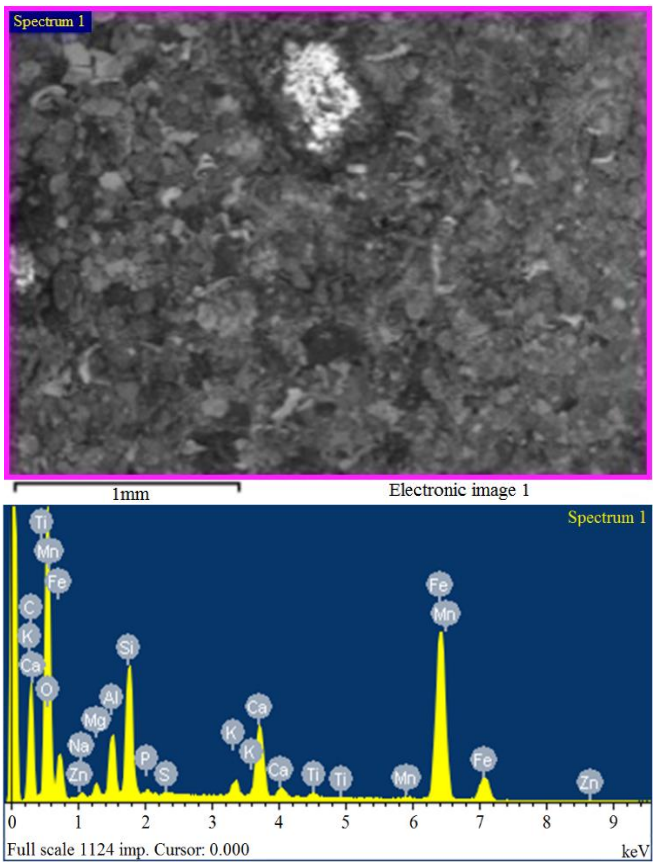

Element, Weight (%): C, 2.90; O, 37.02; Si, 0.27; S, 3.01; Ca, 19.4; Mg, 14.08; Fe, 23.32; Total, 100.00

Figure 6. CSD on the inner surface of the pipe formed by the heat carrier in well №3 at a distance of 3 km

Figures 1-6 show the composition of scale formed by water from different sources. To reduce absolute corrosivity, we recommend using inhibitors. Studies on the composition of inhibitors to reduce the aggressiveness of water will be presented in a separate article.

4. DISCUSSION

Proceeding from the experimentally determined indicators of the composition of water from different wells, we concluded with a high probability that the main cause of absolute corrosiveness is a high concentration of sulfate, calcium, and magnesium ions. Since the concentration of the ions differs from well to well, the corrosion aggressiveness of water from different wells varies.

Numerous ways of determining the composition of water serving as a heat carrier in heat supply systems are given in studies, showing the role of Mg^{2+}, Ca^{2+}, and Fe^{2+} ions capable of forming the foci of solid phase – CSDs on the inner surface of metal pipes. CSDs make it difficult for water to circulate through the system, causing additional heating and, in the event of a burst pipe, equipment repair costs.

The composition of water in the heating system in the Turkestan region and the city of Shymkent was our research object. The water composition indicators obtained using chemical analysis were analyzed to identify the potential for CSD formation (Figures 1-6). Using the circulation mode, we tested pipes with water with the established composition flowing over their surface. Figures 1-6 show the weight composition of CSDs and their appearance. The analysis of water composition parameters across different wells allowed us to conclude with a high probability what metal and nonmetal ions in the composition of the water were the cause of CSD formation. Since the concentration of Mg^{2+}, Ca^{2+}, and Fe^{2+} ions varied across the wells, the composition of CSD differed, dense in some places and loose in others.

To prevent the formation of CSD on the surface of a metal pipe, it is necessary to use inhibitors to form a protective film and prevent pipe corrosion. Our findings are the next step in our studies on selecting effective inhibitors. Our results are of practical significance for preserving metal equipment from the effects of corrosion processes. Most importantly, they will help to save energy for additional heating.

Several studies have similarly identified the role of mineral ions, particularly calcium and magnesium, in fostering the growth of crystalline deposits on metal surfaces within heat supply systems [21]. For example, Liu et al. [22] described similar mechanisms where Ca^{2+} and Mg^{2+} ions promote scale formation, which aligns closely with our observations. However, our study provides more specific insights into the role of ions from distinct regional wells, an area that has received limited attention in the literature.

Moreover, recent advances in the use of CCEP and advanced organic inhibitors, such as amino-borates [23], have shown promising results in minimizing the accumulation of such deposits. Comparing these findings with our chemical analysis suggests that while inhibitors remain effective, newer technologies like CCEP may offer a more environmentally friendly and cost-effective alternative to traditional chemical treatments, particularly in highly mineralized waters such as those studied in this paper.

While previous research has explored inhibitors and electrochemical methods such as CCEP, our study emphasizes the need to adapt these technologies to the unique chemical profiles observed in our samples [24, 25]. This localized approach, combined with a detailed chemical breakdown of the scale deposits, represents a novel application of traditional and modern analysis techniques to the field of corrosion science.

5. CONCLUSIONS

1. Studies were conducted to determine the key indicators

of the composition of water from various sources in terms of the content of components causing water aggressiveness.

2. Corrosion and scale compositions formed by water from different sources were established, and their elemental composition was presented.

3. The quantitative and qualitative content of all constituent components of water from the wells capable of forming corrosion-scaling compounds was established using chemical analysis.

4. The study showed the presence of SO^{42-}, Ca^{2+}, and Mg^{2+} ions in the water from wells №1 and 2, which caused the high aggressiveness of this water.

5. The results can be recommended to city and regional municipal utilities and private boiler houses.

ACKNOWLEDGMENTS

This study was funded by the Science Committee of the Ministry of Science and Higher Education of the Republic of Kazakhstan (Grant No.: AP19679027).

REFERENCES

[1] Reizin, B.L., Strizhevskii, I.V., Shevelev, F.A. (1979). Corrosion and Protection of Public Water Supply Systems. Stroiizdat, Moscow.

[2] Akolzin, P.A. (1988). Preventing the Corrosion of Technical Water and Heat Supply Equipment. Metallurgiia, Moscow.

[3] Zhuk, N.P. (2014). Corrosion Theory and the Protection of Metals. Alians, Moscow.

[4] Antoshkin, E.V., Katts, N.V., Vadivaso, D.G. (1966). Metal Spraying. Metallurgiia, Moscow.

[5] Proskurin E.V., Gelovani, V.A., Sonk, A.N. (2017). Diffuse Zinc Coatings: Properties and Applications. Mashinostroenie, Moscow.

[6] Gao, Y., Pastrana, A.P.C., Manogharan, G., van Duin, A.C. (2021). Molecular dynamics study of melting, diffusion, and sintering of cementite chromia core–shell particles. Computational Materials Science, 199: 110721. https://doi.org/10.1016/j.commatsci.2021.110721

[7] Maltanava, H., Stojadinovic, S., Vasilic, R., Karpushenkov, S., Belko, N., Samtsov, M., Poznyak, S. (2023). Photoluminescent coatings on zinc alloy prepared by plasma electrolytic oxidation in aluminate electrolyte. Coatings, 13(5): 848. https://doi.org/10.3390/coatings13050848

[8] Method to remove scale from heat exchange equipment. Patent No.: RU2449234C2. https://patents.google.com/patent/RU2449234C2/ru

[9] Reda, S.M.A.M., Mutasher, D.G., Hasan, W.K., Majdi, H.S., Alderoubi, N. (2024). Enhancing thermal efficiency in solar water heaters: The role of reflective walls. Mathematical Modelling of Engineering Problems, 11(4): 893-902. https://doi.org/10.18280/mmep.110406

[10] Yifei, G., Zhicheng, X., Siyuan, G., Jianyi, L., Hao, X., Xing, X., Xian, G., Wei, Y. (2022). Practical optimization of scale removal in circulating cooling water: Electrochemical descaling-filtration crystallization coupled system. Separation and Purification Technology, 284. https://doi.org/10.1016/j.seppur.2021.120268

[11] Salman, H.S., Mansour, M.M., Lafta, A.M., Shkarah, A.J. (2024). Modification design and process of pipeline to reduce erosion rate and deposited. International Journal of Computational Methods and Experimental Measurements, 12(2): 165-173. https://doi.org/10.18280/ijcmem.120206

[12] Murphy, S., Vynnycky, M., Mitchell, S.L., O'Kiely, D. (2023). Reaction dynamics and early-time behaviour of chemical decontamination. IMA Journal of Applied Mathematics, 88(5): 765-804. https://doi.org/10.1093/imamat/hxae001

[13] Elistratova, Y., Seminenko, A., Uvarov, V., Scherbinina, O. (2023). The economic aspect of the scale-forming dignostics layers in plate heat exchangers. Bulletin of Belgorod State Technological University Named after. V. G. Shukhov, 8(5): 42-51. https://doi.org/10.34031/2071-7318-2023-8-5-42-51

[14] Liu, H.X., Jin, Z.Y., Wang, Z., Liu, H.F., Meng, G.Z., Liu, H.W. (2023). Corrosion inhibition of deposit-covered X80 pipeline steel in seawater containing Pseudomonas stutzeri. Bioelectrochemistry, 149: 108279. https://doi.org/10.1016/j.bioelechem.2022.108279

[15] Mohamed, A., Martin, U., Visco, D.P., Townsend, T., Bastidas, D.M. (2023). Interphase corrosion inhibition mechanism of sodium borate on carbon steel rebars in simulated concrete pore solution. Construction and Building Materials, 408. https://doi.org/10.1016/j.conbuildmat.2023.133763

[16] Zaidi, K., Bouroumane, N., Merimi, C., Aouiniti, A., Touzani, R., Oussaid, A., Hammouti, B., Salim, R., Kaya, S., Ibrahim, S.M. (2023). Iron-ligand complex, an efficient inhibitor of steel corrosion in hydrochloric acid media. Journal of Molecular Structure, 1284: 135434. https://doi.org/10.1016/j.molstruc.2023.135434

[17] Bijapur, K., Molahalli, V., Shetty, A., Toghan, A., De Padova, P., Hegde, G. (2023). Recent trends and progress in corrosion inhibitors and electrochemical evaluation. Applied Sciences, 13(18): 10107. https://doi.org/10.3390/app131810107

[18] Avdeev, Y.G., Kuznetsov, Y.I. (2023). Organic inhibitors of metal corrosion in acid solutions. I. mechanism of protective action. Russian Journal of Physical Chemistry A, 97(3): 413-427. https://doi.org/10.1134/S0036024423030056

[19] Sarma P.K., Konijeti R., Subramanyam T., Prasad L.S.V., Korada V.S., Srinivas V., Vedula D.R., Prasad V.S.R.K. (2017). Fouling and its effect on the thermal performance of heat exchanger tubes. International Journal of Heat and Technology, 35(3): 509-519. https://doi.org/ 10.18280/ijht.350307

[20] Sun, L., Yan, W.P. (2018). Prediction of wall temperature and oxide scale thickness of ferritic–martensitic steel superheater tubes. Applied Thermal Engineering, 134: 171-181. https://doi.org/10.1016/j.applthermaleng.2018.01.127

[21] Gong, M., Yang, X., Li, Z., Yu, A., Liu, Y., Guo, H., Li, W., Xu, S., Xiao, L., Li, T., Zou, W. (2024). Surface engineering of pure magnesium in medical implant applications. Heliyon, 10(11): e31703. https://doi.org/10.1016/j.heliyon.2024.e31703

[22] Liu, J., Zhou, F., Dai, Q., Gao, H. (2021). Effect of Ca^{2+},

Mg^{2+}, Ba^{2+} and Sr^{2+} cations on calcium carbonate scaling formation in oil-gas well: Based on density functional theory study and molecular dynamics simulation. Journal of Crystal Growth, 563: 126089. https://doi.org/10.1016/j.jcrysgro.2021.126089

[23] Bolan, S., Wijesekara, H., Amarasiri, D., Zhang, T., Ragályi, P., Brdar-Jokanović, M., Rékási, M., Lin, J.Y., Padhye, L.P., Zhao, H., Wang, L., Rinklebe, J., Wang, H., Siddique, K.H.M., Kirkham, M.B., Bolan, N. (2023). Boron contamination and its risk management in terrestrial and aquatic environmental settings. Science of The Total Environment, 894: 164744. https://doi.org/10.1016/j.scitotenv.2023.164744

[24] Kang, R., Zhao, Y., Hait, D., Gauthier, J.A., Kempler, P.A., Thurman, K.A., Boettcher, S.W., Head-Gordon, M. (2024). Understanding ion-transfer reactions in silver electrodissolution and electrodeposition from first-principles calculations and experiments. Chemical Science, 15(13): 4996-5008. https://doi.org/10.1039/D3SC05791G

[25] Kumar, R., Singh, R., Dutta, S. (2024). Review and outlook of hydrogen production through catalytic processes. Energy & Fuels, 38(4): 2601-2629. https://doi.org/10.1021/acs.energyfuels.3c04026